Available online at www.sciencedirect.com

SciVerse ScienceDirect

Scripta Materialia 68 (2013) 937–940

Scripta MATERIALIA

www.elsevier.com/locate/scriptamat

Exploring grain boundary energy landscapes with the activation-relaxation technique

Kathleen C. Alexander and Christopher A. Schuh*

Department of Materials Science and Engineering, Massachusetts Institute of Technology, 77 Massachusetts Avenue, Cambridge, MA 02139, USA

Received 20 January 2013; revised 13 February 2013; accepted 14 February 2013
Available online 26 February 2013

To develop a structure–kinetic property mapping for grain boundaries requires an understanding of their energy landscapes, i.e. the energy basins and nearby saddle points separating adjacent structures. We implement the activation-relaxation technique to obtain a first view of grain boundary energy landscapes for the Σ5 (130), Σ5 (210) and Σ3 (111) grain boundaries in copper. The energy landscapes of these boundaries are very different, which supports a focus on energy landscapes, rather than absolute boundary energy, to understand boundary properties.

Keywords: Grain boundary energy; Grain boundary migration; Grain boundary sliding; Energy landscape; Simulation

Grain boundaries (GBs) govern many materials properties such as plasticity, intergranular and fatigue cracking, corrosion, creep, and thermal coarsening [1–6]. The kinetic properties of individual GBs that drive such macroscopic behavior can vary by orders of magnitude from one GB to the next [7–10], and, as such, the macroscopic properties of materials are significantly impacted by the collection of individual grain boundaries in a specimen [7,11,12]; the practice of "grain boundary engineering" relies heavily on this concept and has led to some remarkable property enhancements [7,11–13]. However, predictive relationships between GB structure and kinetic properties remain elusive. This is at least in part because the number of possible GB configurations across the full five-parameter GB crystallographic space is vast [14]. Over the years, a number of investigations of GB properties across the five-parameter space have been undertaken [15–18]. However, the major focus of most such work has been on the absolute excess energy of GBs, while the kinetic properties of GBs across the space have been substantially less studied.

It is the premise of our investigation that grain boundary engineering, by virtue of its dependence upon GB kinetic properties, does not necessarily require information about the excess energy of GBs, but rather needs input on the shape and structures of GB energy landscapes—the series of local stable and metastable GB configurations and the pathways and activated states between them. It is the depth or shallowness of the potential well that an individual GB sits in relative to other nearby configurations, rather than the absolute position of that well on the energy scale, that will determine the stability and evolution of a GB. Yet to our knowledge, there are no prior studies revealing the energy landscape of any given GB. It is our purpose here to do so for a few coincidence boundaries to establish the importance of such data for grain boundary engineering.

An illustration of the concept of the GB energy landscape is shown in Figure 1. The atomic configurations of a GB in its absolute minimum energy (ground state) configuration, at a transition state, and at an adjacent minimum are shown, mapped to a schematic potential energy landscape plotted on two arbitrary axes denoting the configuration space. A transition state corresponds to the point of highest energy on a pathway of lowest energy connecting two adjacent minima. While transition states have negative curvature in one direction, minima (or basins) have positive curvature in every direction.

GB potential energy landscapes in this study were investigated using the activation-relaxation technique (ART) [19,20]. ART is an efficient saddle point finding

* Corresponding author. Tel.: +1 617 452 2659; e-mail: schuh@mit.edu

1359-6462/$ - see front matter © 2013 Acta Materialia Inc. Published by Elsevier Ltd. All rights reserved.
http://dx.doi.org/10.1016/j.scriptamat.2013.02.038

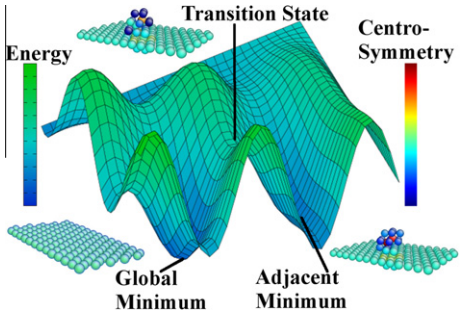

Figure 1. Schematic of a potential energy landscape of a grain boundary. Atomic configurations of the Σ3 (1 1 1) grain boundary modeled in copper are shown as examples of grain boundary configurations at the indicated points of interest. The potential energy surface shown here is intended as a visual aide and is plotted as energy vs. a two-dimensional projection of configuration space. Atomic configuration images were generated with AtomEye [30].

algorithm consisting of three phases: perturbation, convergence and relaxation. The initial grain boundary configurations were generated, using the LAMMPS molecular dynamics simulation package [21,22], from two individual grains oriented according to the desired final configuration and separated by a small distance of ~1 Å. Using the embedded atom method [23] potential developed by Mishin et al. [24,25], a conjugate gradient minimization was performed on the two-grain system, resulting in a minimum energy GB configuration. The conjugate gradient relaxation was performed at zero pressure in a region within a cutoff distance of the boundary. In some cases, numerous initial configurations were required in order to generate the ground state structure. Three symmetric tilt GBs were investigated here:

- Σ5 (1 3 0) (905 mJ m^{-2}, 3232 atoms)
- Σ5 (2 1 0) (952 mJ m^{-2}, 2040 atoms)
- Σ3 (1 1 1) coherent twin (23 mJ m^{-2}, 5850 atoms)

System size and GB-region cutoff were optimized in the initial stages of the investigation by considering systems ranging from less than 1000 atoms to greater than 10,000, and varying the GB-region cutoff distance.

The present implementation of ART was initiated by perturbing a random GB atom, identified as one with a centrosymmetry parameter greater than 4.0 [22,26], by a distance $\alpha_o = 1.3$ Å in a random direction. The perturbation phase followed Ref. [27], with $N_R = 2$ steps of modified conjugate gradient relaxation for each perturbation, and $\lambda_c = -1.0$, the cutoff value the minimum eigenvalue had to be less than in order to proceed to the convergence phase of the algorithm. The lowest eigenvalue of the system was calculated using the Lanczos algorithm with $L_N = 15$ Lanczos iterations, where the product of the Hessian matrix with the jth vector of the Krylov subspace was calculated using a second-order finite-difference approximation. If, after L_N Lanczos iterations, the residual (i.e. the difference $|Av-\lambda v|$ for a matrix A, eigenvalue λ and approximate eigenvector v) was greater than 0.1, the Lanczos algorithm was implicitly restarted using the most recently approximated eigenvector as the initial guess until the residual was less than 0.1 or the Lanczos method had been attempted L_N times [28]. The convergence phase again followed Ref. [27] with $\alpha_{max} = 0.5$ Å, the largest distance any atom could move for a given convergence step, $f_{tol} = 0.005$ eV $Å^{-1}$, the maximum value any component of the force vector could have for a transition state to be identified, and $N_{max} = 50$–75, the maximum number of convergence steps.

The requirements for successful saddle point identification were $\lambda_{min} \leqslant \lambda_{cf} = -0.001$ and $f_{max} \leqslant f_{tol}$. If these were satisfied, the connectivity checking phase of the algorithm was entered. Following Ref. [27], connectivity was verified if a constant strain conjugate gradient minimization of the saddle point configuration resulted in a maximum deviation from the initial configuration, $\Delta x_{max} \leqslant \Delta x_{tol} = 0.5$ Å. The adjacent minima to connected saddle points were identified using a conjugate gradient minimization in LAMMPS with all stress components zero. Transitions for which the adjacent minimum was sufficiently similar to the saddle point (within 0.05 eV of the saddle point energy and with $\Delta x_{max} \leqslant \Delta x_{tol}$) were excluded as these are not kinetically viable pathways.

As the algorithm ran, saddle points were binned into groups of five according to the order in which they were found, and frequencies and standard deviations of their occurrence were determined. The t-statistic was then used to calculate the total number of saddle points required to achieve a desired confidence interval (95%, two-sided, within 10% of the true mean) for the frequency of each saddle point. If the number of saddle points found was greater than what was required for the confidence interval for the most frequently occurring saddle point, the program was stopped, and the space was deemed sufficiently explored.

It should be noted that the choice of parameters used in ART, most importantly α_o and λ_c, can affect the distribution of saddle points found in the search; however, we have found that the specific transitions revealed are independent of these parameters, with the exception of very extreme choices. For this reason, parameters that minimized the time required to find a saddle point were used.

The present implementation of ART was validated through investigation of vacancy migration in copper, yielding excellent agreement with expectations (i.e. a single prominent event with activation energy of 0.68 eV, compared to 0.71 eV from experiments and within 0.01 eV of other simulation results for copper [24]). The precision of the saddle points found by the algorithm was thus taken to be 0.01 eV, limited by f_{tol}, while the accuracy was limited by the potential used and was taken to be 0.03 eV. As our interest is in energy differences rather than absolute energies, the precision drives the uncertainty in this investigation.

From the output of ART, the energy landscapes governing the kinetic behavior of GBs are obtained, and a graphical representation of this data is shown in Figure 2 for the three GBs studied here. The nodes of each graph correspond to accessible states (minima and transition states) and are positioned with respect to the vertical energy axes shown. Multiple nodes with very similar energy were combined together to generate the pictorial representation in Figure 2 and are larger in size than